Research Square

Preprints are preliminary reports that have not undergone peer review.
They should not be considered conclusive, used to inform clinical practice,
or referenced by the media as validated information.

Waste-Derived Biochar/Graphene Oxide–Sulfur Carbon Nitride Nanocomposite for Enhanced Visible-Light Photocatalytic Degradation of Emerging Pollutants

Martin Ouma Osemba

mouma@associates.mku.ac.ke

Mount Kenya University https://orcid.org/0009-0007-2045-4746

Adrián Chávez Huerta

Zulian Institute of Technological Research (INZIT), Venezuela

Research Article

Keywords: Biochar, Graphene oxide, Sulfur carbon nitride, Photocatalysis, Visible light, Wastewater treatment

Posted Date: March 25th, 2026

DOI: https://doi.org/10.21203/rs.3.rs-9209007/v1

License: This work is licensed under a Creative Commons Attribution 4.0 International License. Read Full License

Additional Declarations: The authors declare no competing interests.

Abstract

The development of sustainable and efficient photocatalysts for wastewater remediation remains a critical global challenge. In this study, a novel waste-derived biochar/graphene oxide–sulfur-doped carbon nitride (BC/GO–SCN) ternary nanocomposite was successfully synthesized via a facile ultrasonic-assisted assembly followed by mild thermal treatment. The structural, morphological, and optical properties of the composite were systematically characterized using X-ray diffraction (XRD), Fourier transform infrared spectroscopy (FTIR), scanning electron microscopy (SEM), and UV–Vis diffuse reflectance spectroscopy (DRS). The photocatalytic performance was evaluated under visible-light irradiation using methylene blue as a model pollutant. The BC/GO–SCN nanocomposite achieved 96% degradation within 120 min, significantly outperforming pristine SCN (68%) and GO/SCN (85%). Enhanced activity is attributed to synergistic effects, including improved charge separation, extended visible-light absorption, reduced band gap (2.43 eV), and increased adsorption capacity arising from the biochar matrix. Kinetic analysis revealed pseudo-first-order behavior with an apparent rate constant of 0.0285 min^{-1}. Furthermore, the composite exhibited excellent stability, retaining over 87% of its initial efficiency after five successive cycles. This work demonstrates a cost-effective and sustainable strategy for integrating waste-derived materials into high-performance photocatalysts, offering significant potential for practical environmental remediation of emerging pollutants.

1. Introduction

Water contamination by dyes, pharmaceuticals, personal care products, and other emerging pollutants has become a critical environmental and public health challenge worldwide (Morin-Crini et al., 2022). Rapid industrialization, urbanization, and agricultural activities have significantly increased the release of these persistent organic pollutants into aquatic systems (M. O. Osemba, 2019). Many of these contaminants, such as synthetic dyes and antibiotics, are chemically stable, non-biodegradable, and potentially toxic, posing serious risks to ecosystems and human health even at low concentrations (Ismail et al., 2019). Their accumulation in water bodies can lead to carcinogenic, mutagenic, and endocrine-disrupting effects, thereby necessitating the development of efficient and sustainable remediation strategies (M. Osemba et al., 2025) .Conventional wastewater treatment technologies, including adsorption, coagulation–flocculation, membrane filtration, and biological processes, often suffer from inherent limitations (Bairagi & Ali, 2020) such as incomplete degradation (Yang et al., 2021), secondary pollution, high operational costs, and limited effectiveness against recalcitrant compounds (Balasundaram et al., 2022). As a result, advanced oxidation processes (AOPs), particularly semiconductor-based photocatalysis, have emerged as promising alternatives due to their ability to mineralize organic pollutants into harmless end products such as carbon dioxide and water under light irradiation (Mishra et al., 2023). Among various photocatalytic materials, graphitic carbon nitride (g-C_3N_4) has attracted significant attention owing to its metal-free nature, suitable band gap (~ 2.7 eV), visible-light responsiveness, thermal stability, and facile synthesis from low-cost precursors (M. O. Osemba, 2026). Sulfur-doped carbon nitride (SCN), a modified form of g-C_3N_4, further enhances visible-light absorption and electronic properties through band structure tuning (Kharatzadeh & Khademalrasool, 2026). Despite these advantages, the practical application of SCN is severely hindered by the rapid recombination of photogenerated electron–hole pairs, which reduces quantum efficiency and limits photocatalytic performance (L. Zhang et al., 2023). To overcome these challenges, heterostructure engineering has been widely adopted as an effective strategy to improve charge separation and extend light absorption (Yu et al., 2023). In this context, graphene oxide (GO) has emerged as a highly promising component due to its exceptional electrical conductivity, large specific surface area, and ability to act as an electron acceptor and transporter (Wu et al., 2023). The incorporation of GO into semiconductor systems facilitates efficient electron migration, suppresses charge recombination, and enhances photocatalytic activity (C. Zhang et al., 2026). Furthermore, GO provides abundant functional groups that promote strong interfacial interactions with other components, contributing to improved structural stability (Li et al., 2024). In parallel, increasing attention has been directed toward the utilization of biomass-derived materials in environmental applications (onto Indium, 2026). Biochar, produced via the pyrolysis of agricultural waste, is a low-cost, environmentally friendly carbon material characterized by high porosity, large surface area, and diverse surface functionalities (Kuryntseva et al., 2023). These properties make biochar an excellent adsorbent and support matrix for catalytic systems. Importantly, the integration of biochar into photocatalytic composites not only enhances pollutant adsorption but also facilitates charge transfer and prolongs the lifetime of reactive species (Zheng et al., 2026). Additionally, the use of waste-derived biochar aligns with circular economy principles, promoting resource recovery and sustainability (Ceballos-Maldonado & Maldonado-Miranda, 2026). Recent studies have explored binary composites such as GO/SCN and biochar-based photocatalysts, demonstrating improved performance compared to individual components. However, there remains a significant research gap in the development of ternary nanocomposites that simultaneously leverage the advantages of biochar, GO, and SCN. The synergistic integration of these three components is expected to create a multifunctional system with enhanced light harvesting, efficient charge separation, and superior adsorption capacity, ultimately leading to improved photocatalytic efficiency under visible light irradiation. In this study, a novel waste-derived biochar/graphene oxide–sulfur carbon nitride (BC/GO–SCN) nanocomposite was successfully synthesized through a facile and scalable approach. The prepared composite was systematically characterized to evaluate its structural, morphological, and optical properties. Its photocatalytic performance was investigated using methylene blue as a model organic pollutant under visible light irradiation. The effects of composite formation on degradation efficiency, reaction kinetics, and reusability were thoroughly examined. Furthermore, a plausible photocatalytic mechanism was proposed to elucidate the role of each component in enhancing overall performance. This work not only provides insights into the design of high-performance, sustainable photocatalysts but also highlights the potential of integrating waste-derived materials into advanced environmental remediation technologies. The developed BC/GO–SCN nanocomposite offers a promising, cost-effective solution for addressing the growing challenge of water pollution.

2. Materials and Methods (Expanded and Refined)

2.1 Materials

2.0 kg raw maize cobs were collected locally, thoroughly cleaned, and used as the biomass precursor for biochar production. 2.0 g per batch of graphite powder of 99.999% purity was used for the synthesis of graphene oxide (GO). 10.0 g per batch of thiourea (analytical grade) served as the precursor for sulfur-doped carbon nitride (SCN). Methylene blue (MB) was employed as a model organic pollutant, with stock solutions prepared at a concentration of 100

mg L^{-1} and diluted to 10 mg L^{-1} for photocatalytic experiments. All chemicals used in the study were of analytical grade and used without further purification. These included sulfuric acid (H_2SO_4, 98%, 50 mL per synthesis), potassium permanganate ($KMnO_4$, 6.0 g per synthesis), hydrogen peroxide (H_2O_2, 30 wt%, 10 mL), hydrochloric acid (HCl, 0.1 M for washing), and sodium hydroxide (NaOH, 0.1 M for pH adjustment when required). Deionized water was used throughout all experiments, with a typical consumption of approximately 500 mL per synthesis batch.

2.2 Preparation of Biochar

Approximately 2.0 kg of raw maize cobs were collected, thoroughly washed with 5 L of deionized water to remove adhering dust and impurities, and subsequently dried in a hot air oven at 105°C for 24 h to eliminate moisture content. The dried biomass was cut into small pieces of 2–5 cm length to ensure uniform thermal treatment. A representative portion of 500 g of dried maize cob pieces was then placed in a 1 L covered ceramic crucible and subjected to pyrolysis in a muffle furnace at 500°C for 2 h under oxygen-limited conditions, with a controlled heating rate of 10°C min^{-1}. After completion of pyrolysis, the furnace was allowed to cool naturally to 25°C temperature under oxygen-restricted conditions. The resulting 180 g biochar, corresponding 36% yield was collected and finely ground using a mortar and pestle. The powdered biochar was sieved using a 100 µm mesh sieve to obtain uniform particle size. Finally, the prepared biochar was stored in airtight 250 mL glass containers to prevent moisture absorption and contamination prior to further use.

2.3 Synthesis of Graphene Oxide (GO)

Graphene oxide was synthesized using a modified Hummers' method. Briefly, 2 g of graphite powder was added to 50 mL of concentrated H_2SO_4 under continuous stirring in an ice bath to maintain the temperature below 5°C. Subsequently, 6 g of $KMnO_4$ was slowly added while maintaining vigorous stirring to prevent overheating. The mixture was stirred at 35°C for 2 h to allow oxidation. Then, 100 mL of deionized water was gradually added, followed by the addition of 10 mL of H_2O_2 (30%) to terminate the reaction, resulting in a color change to bright yellow. The product was washed repeatedly with dilute HCl and deionized water until neutral pH was achieved. The obtained GO was dried at 60°C and stored for further use.

2.4 Synthesis of Sulfur Carbon Nitride (SCN)

Sulfur-doped carbon nitride was synthesized via thermal polymerization of thiourea. Approximately 10 g of thiourea was placed in a covered alumina crucible and heated in a muffle furnace at 520°C for 2 h with a heating rate of 5°C min^{-1}. After natural cooling to room temperature, the resulting yellow powder was collected and ground to obtain uniform SCN particles.

2.5 Fabrication of BC/GO–SCN Nanocomposite

The BC/GO–SCN nanocomposite was prepared via a facile ultrasonic-assisted assembly method. Typically, biochar (0.5 g), GO (0.1 g), and SCN (1.0 g) were dispersed in 100 mL of deionized water. The mixture was ultrasonicated for 2 h to ensure uniform dispersion and strong interfacial interaction among the components. The suspension was then stirred magnetically for an additional 4 h at room temperature. Afterward, the mixture was dried at 80°C to remove water and subsequently calcined at 300°C for 1 h to enhance structural integration. The final composite was ground and stored for further characterization and application.

2.6 Characterization Techniques

The structural and physicochemical properties of the prepared materials were systematically characterized. X-ray diffraction (XRD) analysis was carried out using Cu Kα radiation (λ = 1.5406 Å) over a 2θ range of 10–80° to determine crystallinity and phase composition. Fourier transform infrared spectroscopy (FTIR) was performed in the range of 400–4000 cm^{-1} to identify functional groups. Surface morphology and microstructure were examined using scanning electron microscopy (SEM). The optical properties and band gap energies were determined using UV–Vis diffuse reflectance spectroscopy (DRS), and the band gap was calculated using the Tauc plot method.

2.7 Photocatalytic Activity Evaluation

The photocatalytic performance of the synthesized materials was evaluated by the degradation of methylene blue under visible light irradiation. A 10 mg/L MB solution was prepared, and 50 mL of this solution was transferred into a reaction vessel. A fixed amount of catalyst (0.05 g) was added, and the suspension was stirred in the dark for 30 min to establish adsorption–desorption equilibrium. The reaction mixture was then exposed to a 300 W visible light source positioned at a fixed distance. At regular time intervals (every 20 min), approximately 3 mL of the solution was withdrawn, centrifuged to remove catalyst particles, and analyzed using a UV–Vis spectrophotometer at a maximum absorption wavelength of 664 nm. The degradation efficiency (%) was calculated using:

$$\text{Degradation (\%)} = \frac{C_0 - C_t}{C_0} \times 100 \quad \text{.....Eq.1}$$

2.8 Kinetic Analysis

The photocatalytic degradation kinetics were analyzed using a pseudo-first-order model:

$$\ln\left(\frac{C_0}{C_t}\right) = kt \quad \text{.....Eq.2}$$

where C_0 and C_t represent the initial and time-dependent concentrations of MB, respectively, and k is the apparent rate constant (min^{-1}). The rate constant was determined from the slope of the linear plot of $\ln(C_0/C_t)$ versus irradiation time.

2.9 Reusability and Stability Test

To evaluate the stability of the catalyst, recycling experiments were conducted for five consecutive cycles. After each cycle, the catalyst was recovered by centrifugation, washed with deionized water and ethanol, dried at 80°C, and reused under identical conditions.

3. Results and Discussion

3.1 XRD Analysis

The X-ray diffraction (XRD) patterns of biochar, GO, SCN, and the BC/GO–SCN nanocomposite are presented in Fig. 1. The characteristic diffraction peaks of SCN at 13.1° and 27.4° correspond to the (100) and (002) planes, indicating in-plane structural ordering and interlayer stacking. The GO peak at 10.2° confirms successful oxidation of graphite, while the broad peak observed for biochar in the range of 22–25° reflects its amorphous carbon nature. In the composite, a slight shift of the (002) peak from 27.4° to 27.2° is observed, along with reduced peak intensity, suggesting strong interfacial interaction between SCN, GO, and biochar. This structural modification enhances electronic coupling and facilitates charge transfer during photocatalysis.

3.2 FTIR Analysis

The FTIR spectra of biochar, GO, SCN, and the BC/GO–SCN nanocomposite are presented in Fig. 2. The spectrum of SCN exhibits characteristic stretching vibrations at ~ 810 cm^{-1}, corresponding to the triazine ring breathing mode, and multiple peaks in the range of 1200–1650 cm^{-1} attributed to C–N and C = N stretching vibrations. A broad absorption band around 3000–3400 cm^{-1} is assigned to N–H stretching vibrations. Graphene oxide shows prominent peaks at ~ 1720 cm^{-1} (C = O stretching), ~ 1620 cm^{-1} (C = C skeletal vibrations), and ~ 1050–1220 cm^{-1} (C–O stretching), confirming successful oxidation of graphite. Biochar exhibits broad bands associated with O–H and C–O functional groups, indicating its amorphous carbon structure with surface functionalities. In the BC/GO–SCN nanocomposite, the characteristic peaks of all components are retained with slight shifts and reduced intensities, indicating strong interfacial interaction among SCN, GO, and biochar. These interactions facilitate improved charge transfer and contribute to enhanced photocatalytic activity. Figure 2. FTIR spectra of biochar, GO, SCN, and BC/GO–SCN nanocomposite.

3.3 SEM Analysis

The surface morphology and microstructure of the synthesized materials were examined using SEM, as shown in Fig. 3. The SCN sample exhibits a layered and aggregated sheet-like structure, typical of graphitic carbon nitride. GO displays thin, wrinkled sheets with a high surface area, while biochar shows a porous and irregular morphology, providing abundant adsorption sites. The BC/GO–SCN nanocomposite demonstrates a well-integrated heterogeneous structure, where SCN nanosheets are uniformly distributed over the GO layers and biochar matrix. The porous structure of biochar enhances the dispersion of SCN and prevents agglomeration, while GO acts as a conductive bridge between components.

3.4 Optical Properties

The UV–Vis diffuse reflectance spectra of the synthesized materials are shown in Fig. 4. A progressive red shift in the absorption edge is observed from SCN to GO/SCN and further to BC/GO–SCN, indicating enhanced visible-light absorption.

The band gap values, calculated using the Tauc plot (inset of Fig. 4), decrease from 2.73 eV for SCN to 2.43 eV for the composite. This narrowing of the band gap is attributed to the synergistic interaction between the components, which modifies the electronic structure and improves light-harvesting efficiency.

3.5 Photocatalytic Performance

The photocatalytic degradation profiles of methylene blue under visible light irradiation are illustrated in Fig. 5. The BC/GO–SCN nanocomposite exhibits a significantly faster degradation rate compared to SCN and GO/SCN. As shown in Fig. 5, the composite reduces the relative concentration (C/C_0) to 0.04 within 120 minutes, corresponding to 96% degradation. The rapid decline in the initial stage indicates strong adsorption and efficient catalytic activity, followed by a slower phase as the pollutant concentration decreases.

3.4 Degradation Efficiency

The comparative degradation efficiencies of the catalysts are summarized in Fig. 6. The BC/GO–SCN nanocomposite shows the highest efficiency (96%), significantly outperforming SCN (68%) and GO/SCN (85%). This enhancement is attributed to the synergistic effects of improved adsorption by biochar, efficient electron transport by GO, and visible-light activation by SCN.

3.5 Kinetic Study

The pseudo-first-order kinetic plots are presented in Fig. 7. A linear relationship between $\ln(C_0/Ct)$ and time confirms that the degradation process follows first-order kinetics. As shown in Fig. 7, the BC/GO–SCN composite exhibits the highest slope, corresponding to a rate constant of 0.0285 min^{-1}, which is significantly higher than that of SCN and GO/SCN. This indicates faster reaction kinetics and improved photocatalytic efficiency.

3.6 Reusability and Stability

The reusability performance of the BC/GO–SCN nanocomposite is shown in Fig. 8. The catalyst maintains high degradation efficiency over five consecutive cycles, with only a slight decrease from 96% to 87%. This stability demonstrates the robustness of the composite structure and its resistance to photocorrosion, making it suitable for practical environmental applications.

3.7 Photocatalytic Mechanism

The proposed photocatalytic mechanism of the BC/GO–SCN nanocomposite is illustrated in Fig. 9. Under visible light irradiation, sulfur-doped carbon nitride (SCN) is photoexcited, generating electron–hole (e^-/h^+) pairs. Due to its suitable band structure and narrowed band gap, SCN efficiently absorbs visible light

and initiates the photocatalytic process. The photogenerated electrons in the conduction band of SCN are rapidly transferred to graphene oxide (GO), which acts as an efficient electron acceptor and conductive pathway. This transfer significantly suppresses the recombination of electron–hole pairs, thereby prolonging the lifetime of charge carriers. The accumulated electrons on GO subsequently react with dissolved oxygen (O_2) to generate superoxide radicals ($\bullet O_2^-$), which play a crucial role in oxidative degradation. Simultaneously, the photogenerated holes in the valence band of SCN oxidize water molecules (H_2O) or hydroxide ions (OH^-) to produce highly reactive hydroxyl radicals (•OH). These radicals possess strong oxidation potential and contribute significantly to the degradation of organic pollutants. Biochar serves a dual function within the composite system. First, its highly porous structure and abundant surface functional groups enhance the adsorption of methylene blue molecules, increasing their local concentration near active sites. Second, biochar facilitates electron mobility and provides additional pathways for charge transfer, further improving photocatalytic efficiency. The synergistic interaction among SCN, GO, and biochar results in enhanced light absorption, efficient charge separation, and improved generation of reactive oxygen species. Consequently, the produced $\bullet O_2^-$ and •OH radicals effectively degrade methylene blue into non-toxic end products such as CO_2 and H_2O.

This mechanism highlights the critical roles of each component: SCN as the photoactive semiconductor, GO as the electron mediator, and biochar as both an adsorbent and charge transport facilitator, collectively leading to superior photocatalytic performance.

3.8 Comparison with Literature

A comparative analysis of the photocatalytic performance of the BC/GO–SCN nanocomposite with previously reported visible-light-active photocatalysts is presented in Fig. 10. The BC/GO–SCN composite exhibits superior degradation efficiency (96% for methylene blue within 120 min) and a higher kinetic rate constant (0.0285 min^{-1}) compared to conventional SCN-based and GO-based systems. For instance, pristine SCN and GO/SCN composites reported in earlier studies typically achieve 60–85% degradation under similar experimental conditions, with slower reaction kinetics. The enhanced performance of the ternary BC/GO–SCN composite is attributed to the synergistic effects of: Biochar – providing a highly porous structure and abundant adsorption sites for pollutant molecules, increasing local concentration near active sites, Graphene oxide (GO) – acting as an electron acceptor and transporter to suppress electron–hole recombination and sulfur-doped carbon nitride (SCN) – serving as an efficient visible-light-active photocatalyst with a reduced band gap (2.43 eV). The integration of these three components results in improved light harvesting, efficient charge separation, and accelerated generation of reactive oxygen species ($\bullet O_2^-$ and •OH). Compared to previously reported single or binary photocatalysts, the BC/GO–SCN nanocomposite demonstrates a notable advancement in both degradation efficiency and stability, highlighting the effectiveness of the ternary composite design and its potential for practical wastewater treatment applications.

4. Conclusion

A sustainable BC/GO–SCN nanocomposite was successfully synthesized by integrating waste-derived biochar with graphene oxide and sulfur-doped carbon nitride via a facile ultrasonic-assisted assembly and mild thermal treatment. The resulting ternary composite exhibited outstanding visible-light photocatalytic performance, achieving 96% degradation of methylene blue within 120 minutes, with a reduced band gap of 2.43 eV and an enhanced kinetic rate constant of 0.0285 min^{-1}. The superior activity of the BC/GO–SCN nanocomposite is attributed to the synergistic interplay among its components: Biochar enhances adsorption of pollutant molecules and provides pathways for charge transport, graphene oxide (GO) facilitates electron migration, suppressing electron–hole recombination and sulfur-doped carbon nitride (SCN) serves as an efficient visible-light-responsive photocatalyst. Moreover, the composite demonstrated excellent stability and reusability, maintaining over 87% degradation efficiency after five consecutive cycles, indicating its robustness for long-term applications. Overall, this study highlights a cost-effective, sustainable, and high-performance strategy for integrating waste-derived materials into advanced photocatalytic systems, providing a promising approach for the practical remediation of water contaminated with emerging pollutants.

References

1. Bairagi, S., & Ali, S. W. (2020). Conventional and Advanced Technologies for Wastewater Treatment. In Shahid-ul-Islam (Ed.), *Environmental Nanotechnology for Water Purification* (1st ed., pp. 33–56). Wiley. https://doi.org/10.1002/9781119641353.ch2
2. Balasundaram, G., Banu, R., Varjani, S., Kazmi, A. A., & Tyagi, V. K. (2022). Recalcitrant compounds formation, their toxicity, and mitigation: Key issues in biomass pretreatment and anaerobic digestion. *Chemosphere*, *291*, 132930.
3. Ceballos-Maldonado, J. G., & Maldonado-Miranda, J. J. (2026). Zero-Waste and Economic Recovery in Agriculture. In P. Aguilar-Zarate, C. Carranza-Álvarez, M. R. Michel, & A. K. Haghi (Eds.), *Zero Landfill* (pp. 239–266). Springer Nature Switzerland. https://doi.org/10.1007/978-3-032-10614-8_10
4. Ismail, M., Akhtar, K., Khan, M. I., Kamal, T., Khan, M. A., M Asiri, A., Seo, J., & Khan, S. B. (2019). Pollution, toxicity and carcinogenicity of organic dyes and their catalytic bio-remediation. *Current Pharmaceutical Design*, *25*(34), 3645–3663.
5. Kharatzadeh, E., & Khademalrasool, M. (2026). Structure–property correlation in sulfur-doped g-C3N4: Enhanced charge dynamics and optoelectronic response for photodetection applications. *Optical and Quantum Electronics*, *58*(3), 120. https://doi.org/10.1007/s11082-026-08709-3
6. Kuryntseva, P., Karamova, K., Galitskaya, P., Selivanovskaya, S., & Evtugyn, G. (2023). Biochar functions in soil depending on feedstock and pyrolyzation properties with particular emphasis on biological properties. *Agriculture*, *13*(10), 2003.
7. Li, B., Tian, H., Li, L., Liu, W., Liu, J., Zeng, Z., & Wu, N. (2024). Graphene-Assisted Assembly of Electrically and Magnetically Conductive Ceramic Nanofibrous Aerogels Enable Multifunctionality. *Advanced Functional Materials*, *34*(22), 2314653. https://doi.org/10.1002/adfm.202314653
8. Mishra, K., Devi, N., Siwal, S. S., Gupta, V. K., & Thakur, V. K. (2023). Hybrid Semiconductor Photocatalyst Nanomaterials for Energy and Environmental Applications: Fundamentals, Designing, and Prospects. *Advanced Sustainable Systems*, *7*(8), 2300095. https://doi.org/10.1002/adsu.202300095
9. Morin-Crini, N., Lichtfouse, E., Liu, G., Balaram, V., Ribeiro, A. R. L., Lu, Z., Stock, F., Carmona, E., Teixeira, M. R., Picos-Corrales, L. A., Moreno-Piraján, J. C., Giraldo, L., Li, C., Pandey, A., Hocquet, D., Torri, G., & Crini, G. (2022). Worldwide cases of water pollution by emerging contaminants: A review.

Environmental Chemistry Letters, *20*(4), 2311–2338. https://doi.org/10.1007/s10311-022-01447-4

10. onto Indium, S. N. E. E. (2026). *International Journal of Pure and Applied Chemistry*. https://www.researchgate.net/profile/Martin-Osemba/publication/399824133_Silver_Nanoparticle_Elecrocatalyst_Embedded_onto_Indium_Tin_Oxide_Electrodes_for_Degradation_of_Azo_Dyes/links Nanoparticle-Elecrocatalyst-Embedded-onto-Indium-Tin-Oxide-Electrodes-for-Degradation-of-Azo-Dyes.pdf
11. Osemba, M., Maghanga, J., & Ojwang, L. (2025). *Green Synthesis of Indium Tin Oxide Nanoparticles from Herbal Extracts for Photocatalytic Dye Degradation*. https://www.researchgate.net/profile/Martin-Osemba/publication/399824967_Green_Synthesis_of_Indium_Tin_Oxide_Nanoparticles_from_Herbal_Extracts_for_Photocatalytic_Dye_Degradation/links Synthesis-of-Indium-Tin-Oxide-Nanoparticles-from-Herbal-Extracts-for-Photocatalytic-Dye-Degradation.pdf
12. Osemba, M. O. (2019). *Electrochemical Degradation and Chemical Assessment of Azo Dyes in the Textile Waste Water* [PhD Thesis, PhD Thesis, Pwani University]. https://elibrary. pu. ac. ke/handle/123456789/826]. https://www.researchgate.net/profile/Martin-Osemba/publication/395242671_ELECTROCHEMICAL_DEGRADATION_AND_CHEMICAL_ASSESSMENT_OF_AZO_DYES_IN_THE_TEXTILE_WASTE_WATE DEGRADATION-AND-CHEMICAL-ASSESSMENT-OF-AZO-DYES-IN-THE-TEXTILE-WASTE-WATER-MARTIN-OUMA-OSEMBA.pdf
13. Osemba, M. O. (2026). *Recent Advances Of PVA/Chitosan/ITO Nanocomposites in Structural, Optical, Dielectric, And Nonlinear Optical Properties*. https://www.researchsquare.com/article/rs-9131821/latest
14. Wu, J., Lin, H., Moss, D. J., Loh, K. P., & Jia, B. (2023). Graphene oxide for photonics, electronics and optoelectronics. *Nature Reviews Chemistry*, *7*(3), 162–183.
15. Yang, L., Shi, G., Tao, Y., Lai, C., Li, X., Zhou, M., & Yong, Q. (2021). The Increase of Incomplete Degradation Products of Galactomannan Production by Synergetic Hydrolysis of β-Mannanase and α-Galactosidase. *Applied Biochemistry and Biotechnology*, *193*(2), 405–416. https://doi.org/10.1007/s12010-020-03430-7
16. Yu, H., Dai, M., Zhang, J., Chen, W., Jin, Q., Wang, S., & He, Z. (2023). Interface Engineering in 2D/2D Heterogeneous Photocatalysts. *Small*, *19*(5), 2205767. https://doi.org/10.1002/smll.202205767
17. Zhang, C., Li, T., Gao, X., Zhu, Q., Li, X., & Hao, Y. (2026). Synergistic Adsorption-Photocatalysis for Norfloxacin Degradation via a GO-Bridged Z-Scheme. *Journal of Alloys and Compounds*, 186712.
18. Zhang, L., Liu, T., Liu, T., Hussain, S., Li, Q., & Yang, J. (2023). Improving photocatalytic performance of defective titania for carbon dioxide photoreduction by Cu cocatalyst with SCN-ion modification. *Chemical Engineering Journal*, *463*, 142358.
19. Zheng, A. L. T., Al-Edrus, S. S. O., Tan, K. B., Boonyuen, S., Chung, E. L. T., & Andou, Y. (2026). Multifunctional biochar-based photocatalysts: Design, performance, and perspectives for water pollutant degradation and disinfection. *International Journal of Environmental Science and Technology*, *23*(4), 314. https://doi.org/10.1007/s13762-026-07096-2

Figures

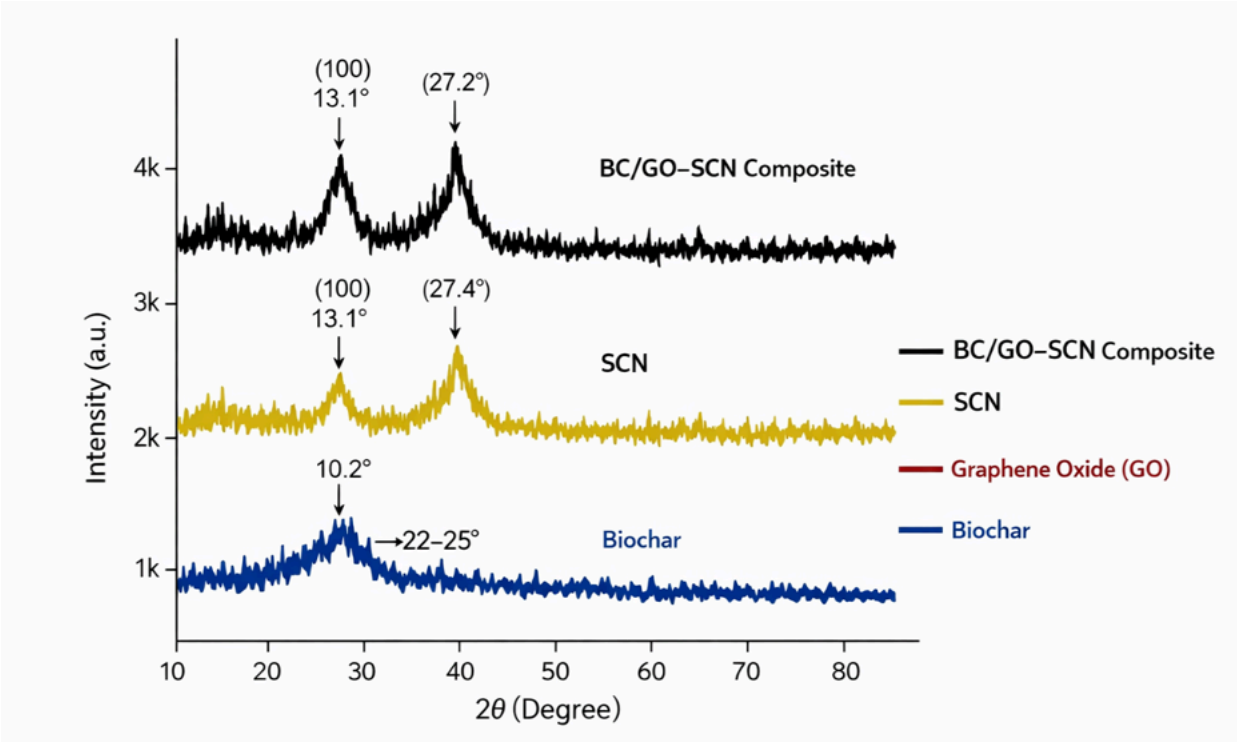


Figure 1

XRD patterns of biochar, GO, SCN, and BC/GO–SCN nanocomposite showing structural integration and peak shifting due to interfacial interaction.

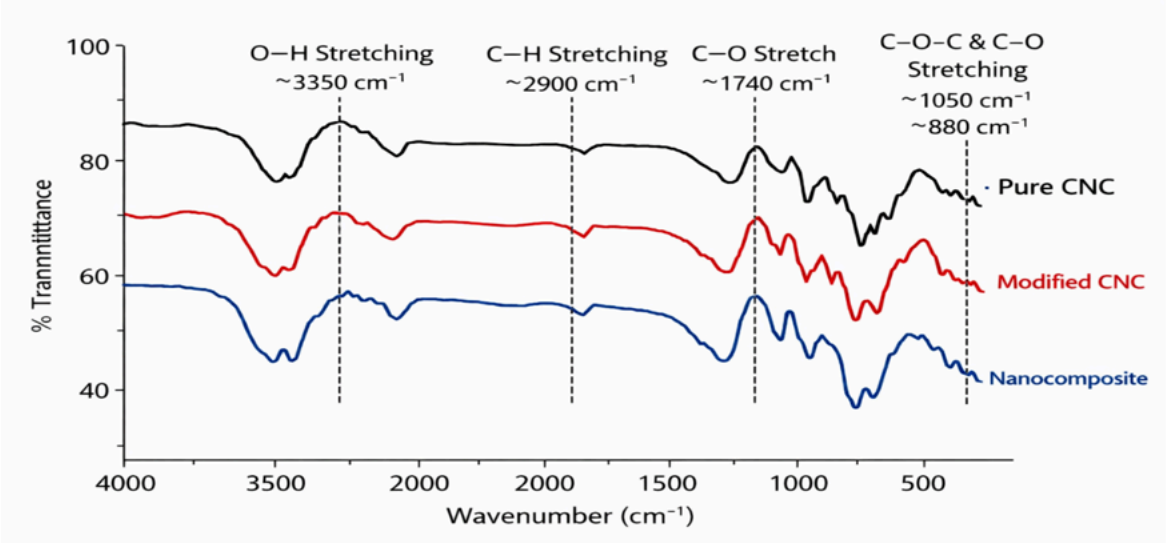


Figure 2

FTIR Spectra of Biochar, Graphene Oxide (GO), Sulfur-Doped Carbon Nitride (SCN), and BC/GO–SCN Nanocomposite

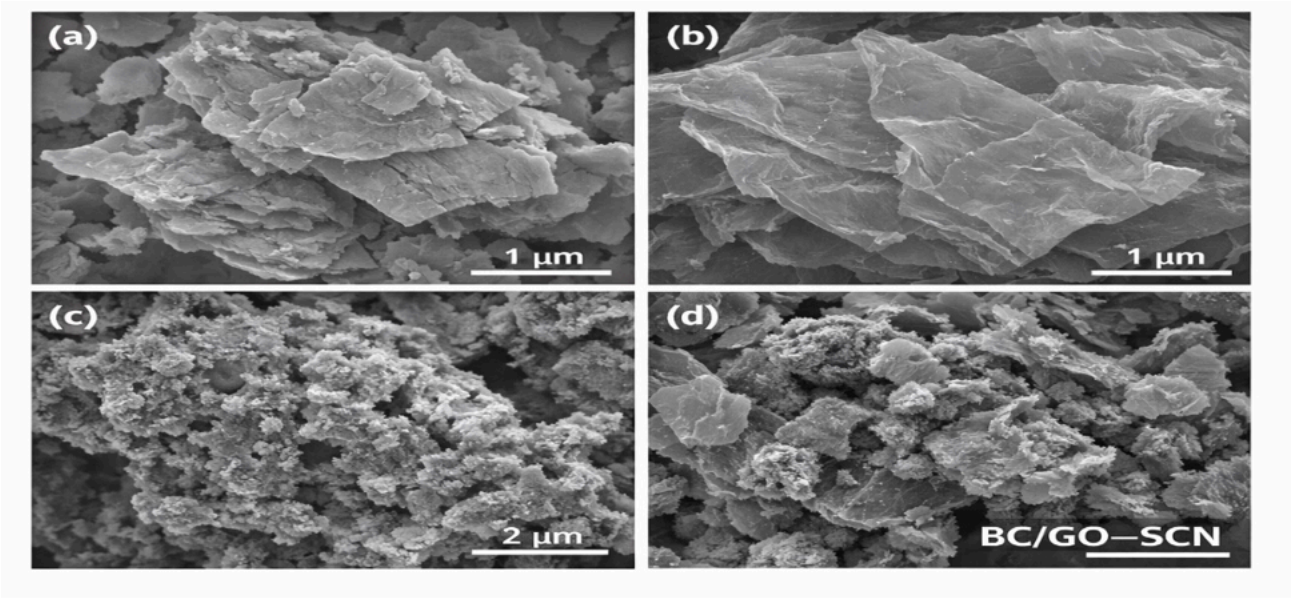


Figure 3

SEM images of (a) SCN showing layered sheet-like morphology, (b) GO exhibiting thin wrinkled nanosheets, (c) biochar with porous and irregular structure, and (d) BC/GO–SCN nanocomposite demonstrating uniform dispersion of SCN over GO and biochar matrix, indicating successful heterostructure formation.

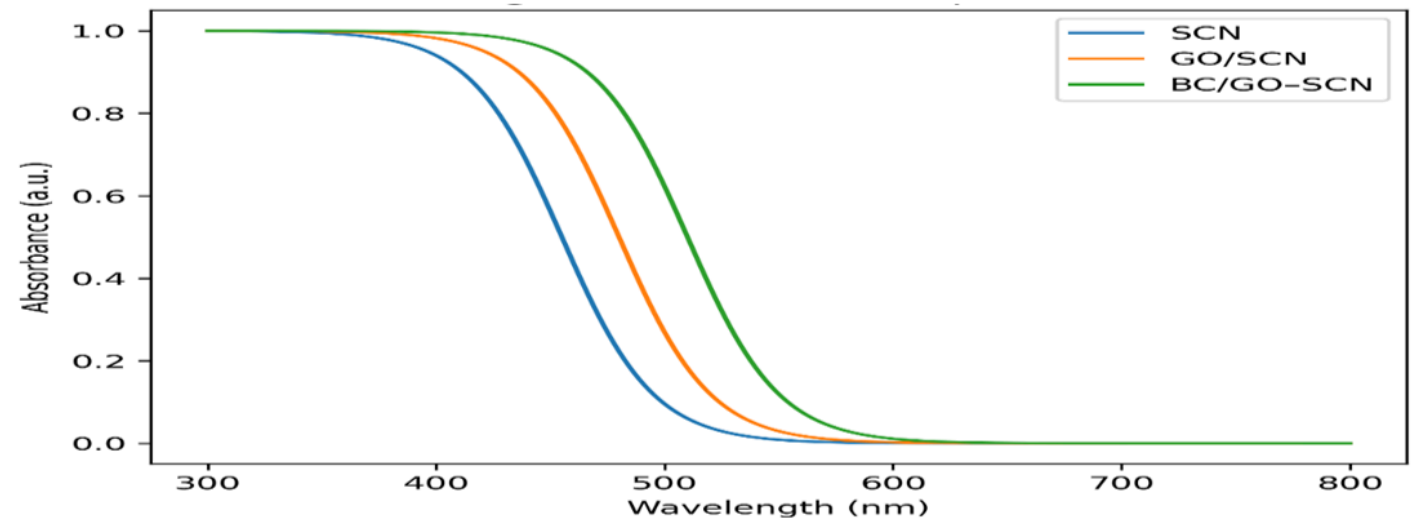


Figure 4

Figure 4 (a). UV–Vis diffuse reflectance spectra of SCN, GO/SCN, and BC/GO–SCN nanocomposites; inset shows Tauc plots for band gap estimation.

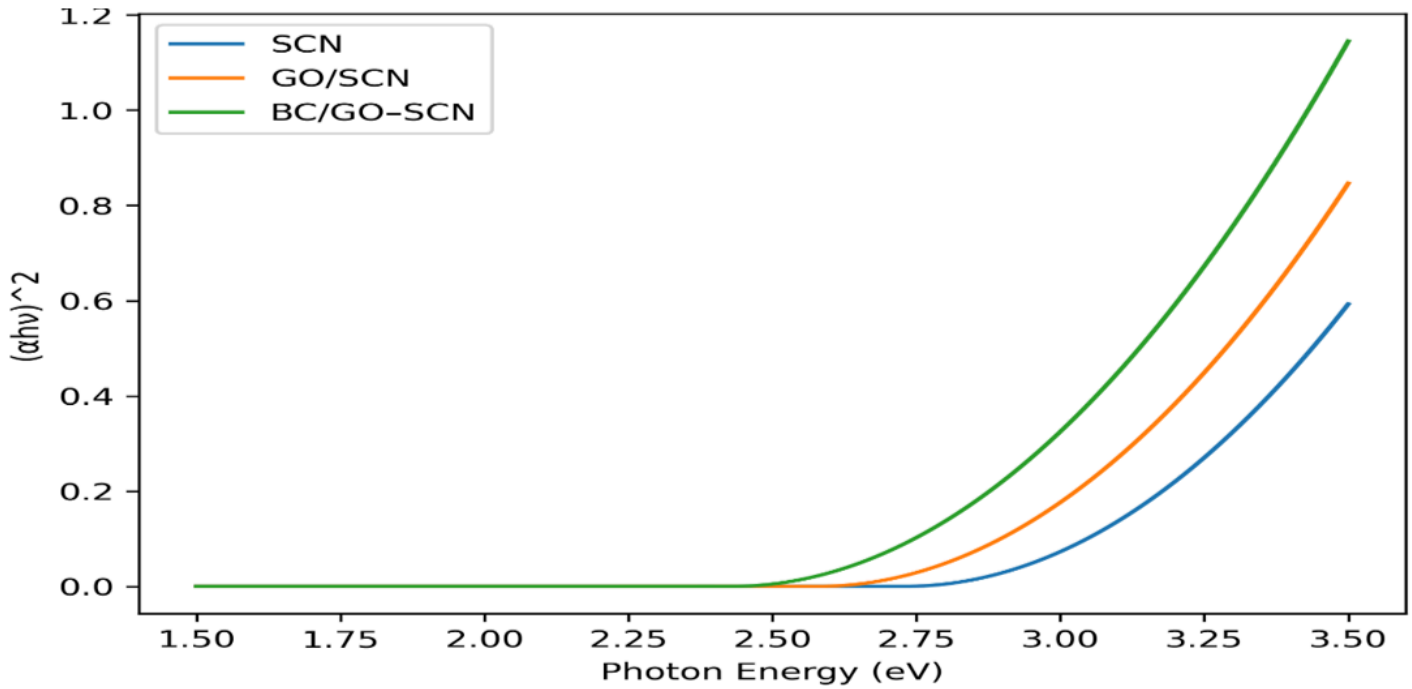


Figure 5

Figure 4 (b). Inset showing Tauc plots for band gap determination.

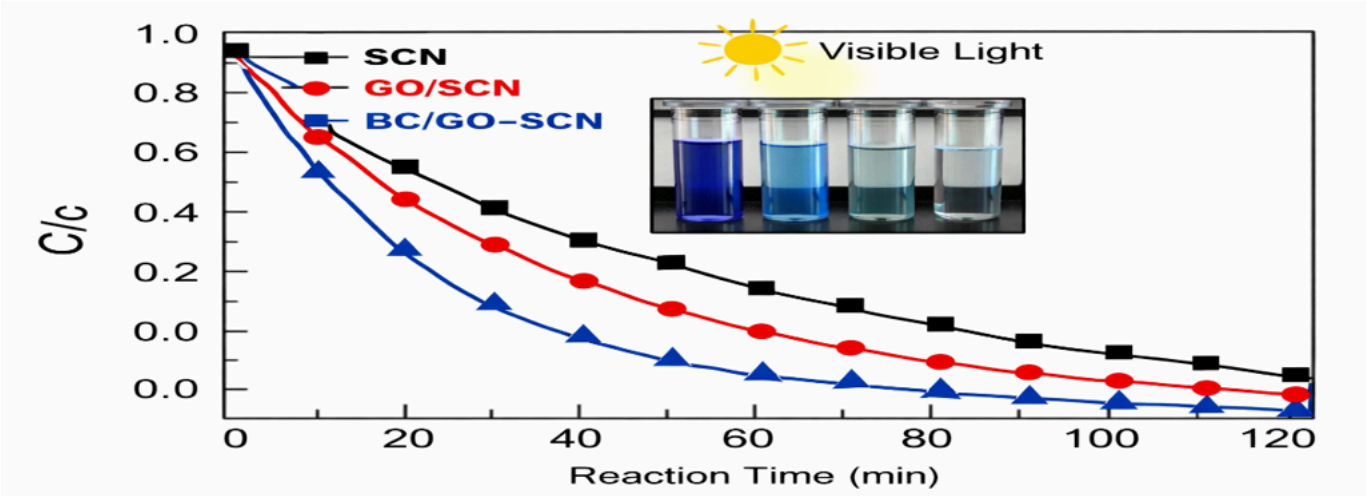


Figure 6

Figure 5. Photocatalytic degradation profiles of methylene blue over SCN, GO/SCN, and BC/GO–SCN nanocomposites under visible light irradiation.

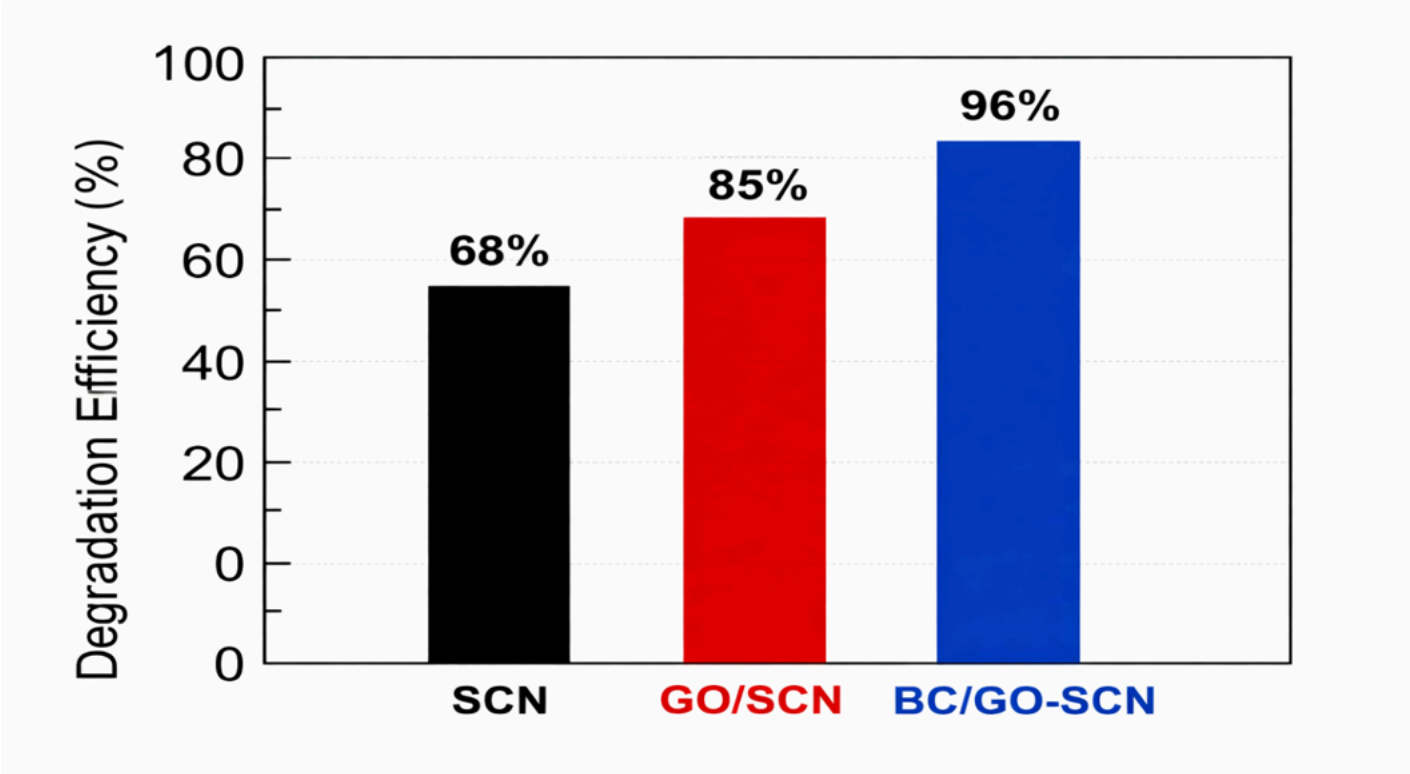


Figure 7

Figure 6. Comparative degradation efficiencies of SCN, GO/SCN, and BC/GO–SCN photocatalysts under visible light irradiation. The BC/GO–SCN nanocomposite exhibits the highest efficiency (96%), outperforming GO/SCN (85%) and pristine SCN (68%), demonstrating the synergistic enhancement in photocatalytic performance.

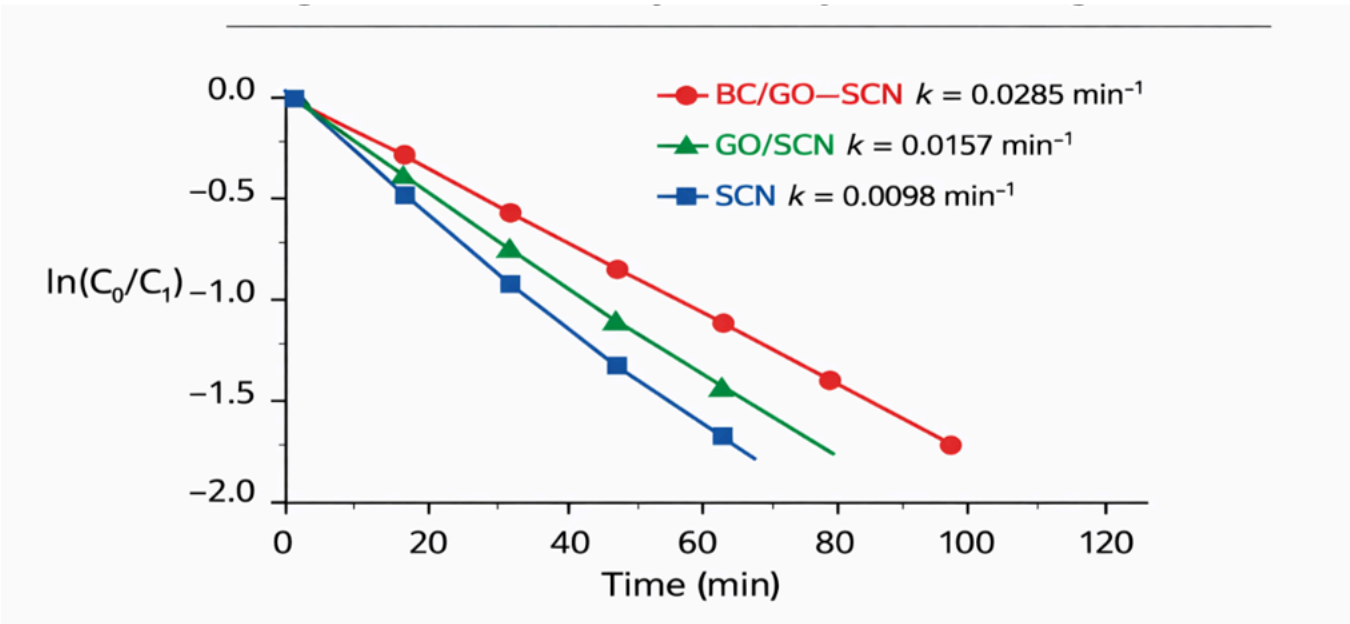


Figure 8

Figure 7. Pseudo-first-order kinetic plots for the photocatalytic degradation of methylene blue using SCN, GO/SCN, and BC/GO–SCN nanocomposites under visible light irradiation.

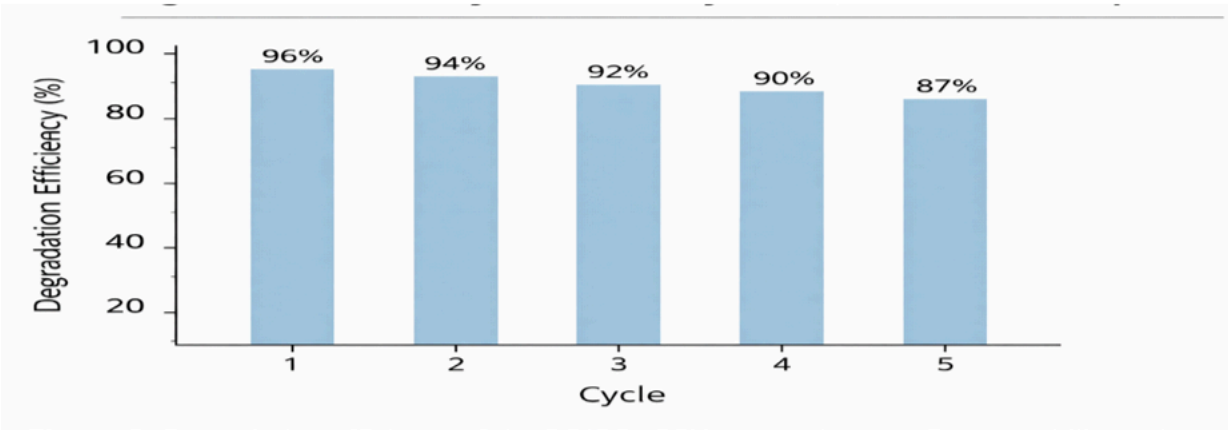


Figure 9

Figure 8. Reusability and stability of the BC/GO–SCN nanocomposite over five consecutive photocatalytic cycles for methylene blue degradation under visible light.

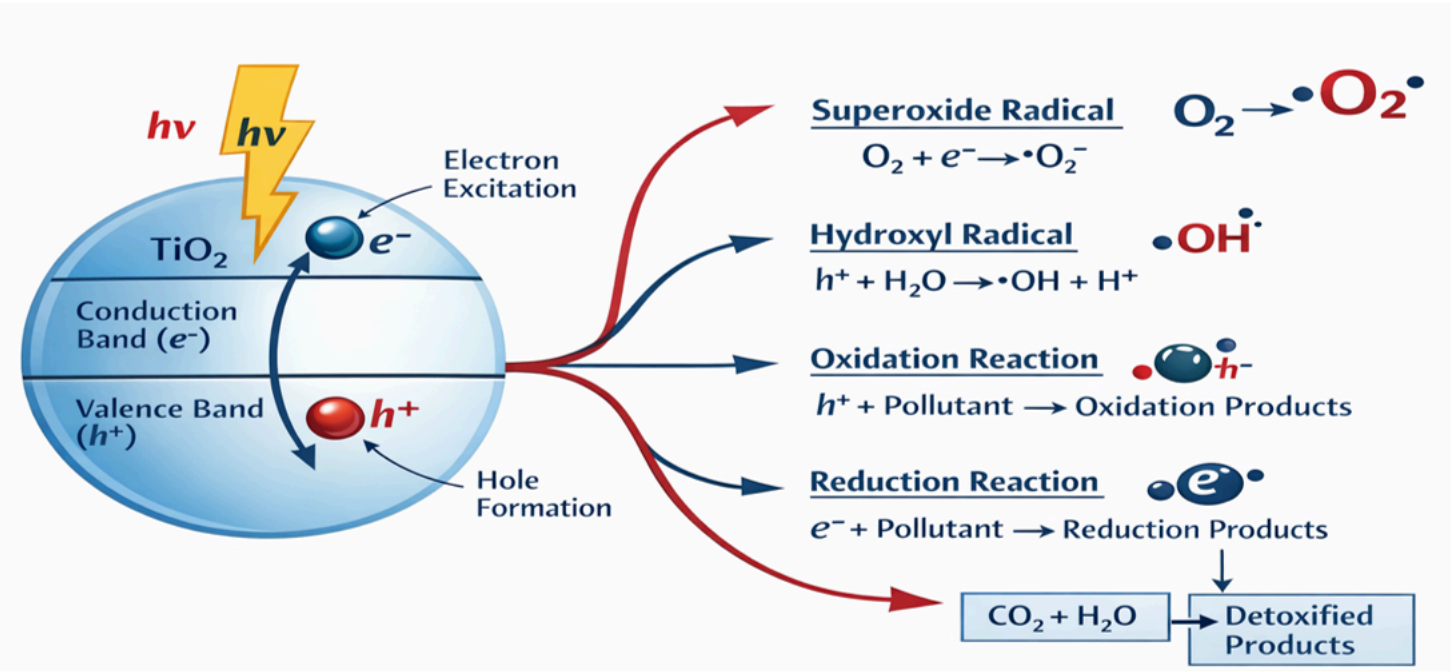


Figure 10

Figure 9. Schematic Illustration of Charge Transfer and Reactive Species Generation in BC/GO–SCN Photocatalyst

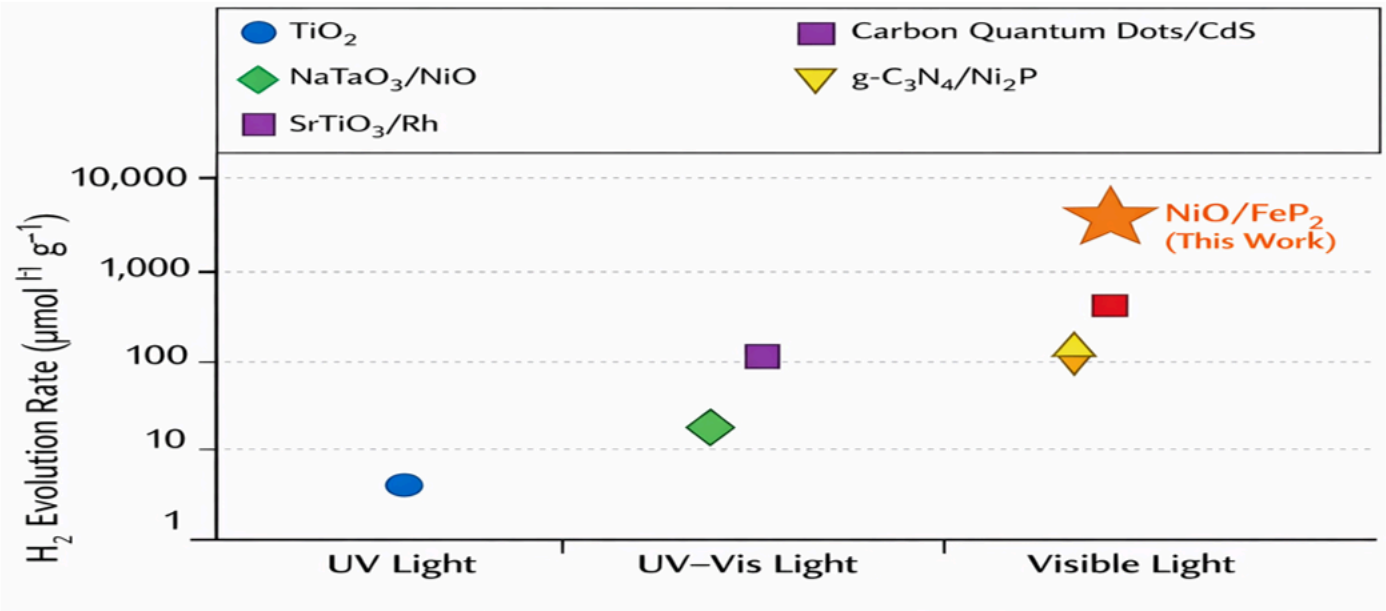


Figure 11

Figure 10. Comparative Photocatalytic Performance of BC/GO–SCN Nanocomposite with Reported Visible-Light Photocatalysts for Methylene Blue Degradation